PNAS RESEARCH ARTICLE | IMMUNOLOGY AND INFLAMMATION

Inflammasome adaptor protein ASC is a mechanistic checkpoint in IL-1β maturation

Giti Saha[a], Pratibha Anchi[a], Richard Wang[a], Alyssa Biondo[b], Sadie Meyer[a], Vinata Kondragunta[a], Larry L. Luchsinger[b], Ismail Syed[c], Humayun Sharif[d], Hao Wu[e,f,1], and Venkat Giri Magupalli[a,1]

Affiliations are included on p. 11.

Contributed by Hao Wu; received December 24, 2025; accepted March 26, 2026; reviewed by Parimal Samir and Junying Yuan

Inflammasome activation triggers caspase-1-dependent maturation of pro-interleukin-1β (pro-IL-1β) in an apoptosis-associated speck-like protein containing a CARD (ASC)-dependent manner, yet the mechanism by which pro-IL-1β is physically recruited to the ASC signaling platform has remained undefined. Here, we identify the ASC linker domain (ASC^{LD}) as a noncanonical protein-interaction interface, that can directly recruits pro-IL-1β onto the ASC speck. Using a live-cell NanoBRET assay, confocal imaging, and pulldown analysis, we show that ASC directly engages pro-IL-1β and that this interaction requires a discrete set of charged residues in the IL-1β mature domain region, forming an ASC-docking surface. Mutagenesis guided by the IL-1β structure confirmed that this interaction is essential for caspase-1-dependent IL-1β maturation but dispensable for pyroptosis. Domain mapping revealed that ASC^{LD}, rather than its N-terminal Pyrin domain (PYD) or C-terminal caspase recruitment domain (CARD), mediates pro-IL-1β recruitment. Using an in-house custom antibody against ASC^{LD}, we show that this region remains exposed within endogenous ASC specks in macrophages. Mutational disruption of ASC^{LD} selectively impaired IL-1β processing in THP-1 cells Mutations disruption data was obtained from THP-1 cells without affecting ASC speck formation or pyroptosis. A cell-penetrating peptide derived from ASC^{LD} selectively blocked pro-IL-1β docking while preserving speck assembly. In 2 mouse models of peritonitis, the blocking peptide uncoupled cytokine maturation from pyroptosis and significantly reduced IL-1β-driven inflammation. Thus, our findings uncover ASC^{LD} as a critical docking interface that positions pro-IL-1β for efficient caspase-1 processing, which adds a mechanistic checkpoint within inflammasomes to license cytokine maturation independently of pyroptotic death. We propose that ASC^{LD} may be a therapeutically tractable node for selective modulation of IL-1β-driven inflammasomopathies.

inflammasomes | IL-1β | pyroptosis

Significance

Inflammasomes are supramolecular complexes that activate caspase-1 and other inflammatory caspases in response to pathogenic and damage stimuli. While inflammasomes play important roles in host defense, their excessive activation leads to hyperinflammation, which induces or exacerbates many human diseases such as cardiovascular, neurodegenerative, and metabolic diseases. One major pathway that inflammasomes regulate inflammation is by converting pro-interleukin-1β (pro-IL-1β) into its mature, inflammatory form in an apoptosis-associated speck-like protein containing a CARD (ASC)-dependent manner. Here, we reveal the mechanism by which the ASC linker domain (ASC^{LD}) acts as a dedicated docking site that recruits pro-IL-1β to the ASC speck for its processing and implicates ASC^{LD} as a potential target strategy for treating IL-1β-driven inflammatory diseases.

The proinflammatory cytokine interleukin-1β (IL-1β) is a central mediator of inflammation whose dysregulated production underlies numerous chronic inflammatory diseases. IL-1β is synthesized as an inactive precursor [pro-interleukin-1β (pro-IL-1β)] in the cytosol and requires proteolytic maturation by caspase-1 within inflammasomes, a supramolecular complex assembled by innate immune sensors in response to infection, injury, and metabolic perturbations (1–3). Inflammasome activation induces apoptosis-associated speck-like protein containing (ASC) a caspase recruitment domain (CARD) nucleation into micron-sized specks that recruit pro-caspase-1 and initiates its autoproteolytic activation (4, 5). Active caspase-1 cleaves pro-IL-1β and pro-IL-18 to their mature forms (6), and also processes gasdermin D (GSDMD) (7–10) inducing pyroptosis, an inflammatory cell death (11–13). While the molecular basis of ASC-mediated caspase-1 recruitment is well established, how pro-IL-1β is physically positioned at the inflammasome for efficient cleavage has remained unresolved. Importantly, *Asc*$^{-/-}$ macrophages fail to cleave pro-IL-1β and pro-IL-18 following NLRC4 inflammasome activation induced by *Salmonella enterica* serovar Typhimurium (14, 15). Although the CARD of NLRC4 can directly recruit pro-caspase-1^{CARD}, and infected cells have active caspase-1 and undergo caspase-1 dependent pyroptosis, pro-IL-1β fail to undergo caspase-1-dependent cleavage and maturation. This finding suggests that inflammasome proteins actively recruit pro-IL-1β to position it near active caspase-1 for cleavage and maturation, indicating that cytokine recruitment is a regulated process rather than a passive, diffusion-limited event.

Here, we identify the ASC linker domain (ASC^{LD}), a flexible region connecting the Pyrin domain (PYD) and CARD, as a docking interface that directly recruits pro-IL-1β to the ASC speck. Using live-cell NanoBRET, confocal imaging, targeted mutagenesis, and biochemical reconstitution, we show that ASC^{LD} remains exposed within endogenous

Reviewers: P.S., The University of Texas Medical Branch; and J.Y., Shanghai Institute of Organic Chemistry.

Competing interest statement: A patent application related to the methods described in this study has been filed by the New York Blood Center.

[1]To whom correspondence may be addressed. Email: wu@crystal.harvard.edu or vmagupalli@nybc.org.

This article contains supporting information online at https://www.pnas.org/lookup/suppl/doi:10.1073/pnas.2537563123/-/DCSupplemental.

Published May 8, 2026.

specks and engages a discrete surface on pro-IL-1β, especially the mature domain. Disruption of this interface selectively abolishes IL-1β maturation in macrophages without impairing ASC speck formation or pyroptosis, delineating a regulatory layer that separates cytokine processing from pyroptosis. Structure–function analysis further identifies specific ASC^{LD} residues, including P97 and P104 as essential for docking, whereas K109 SUMOylation, previously implicated in ASC assembly, is dispensable for cytokine recruitment, indicating that pro-IL-1β engagement operates independently of canonical PYD–PYD or CARD–CARD interactions. We additionally find that a cell penetrating peptide derived from ASC^{LD} blocks pro-IL-1β recruitment and processing while preserving ASC speck formation, thereby uncoupling IL-1β maturation from pyroptosis. The blocking peptide significantly reduces IL-1β-driven inflammation in both mono sodium urate (MSU)-induced and lipopolysaccharide (LPS) + adenosine triphosphate (ATP)-induced peritonitis models in vivo. Together, these findings reveal ASC^{LD} as a noncanonical substrate-recruitment module that spatially organizes pro-IL-1β at the inflammasome, defining a mechanism that govern IL-1β output independently of pyroptotic death.

Results

Direct Recruitment of pro-IL-1β to ASC Speck Enables Spatial Control of pro-IL-1β Maturation. We previously showed that ASC speck is the major site for both caspase-1 activation and pro-IL-1β processing (16). While homotypic CARD–CARD interactions between pro-caspase-1^{CARD} and ASC^{CARD} are known to drive caspase-1 activation on the ASC platform, how pro-IL-1β is recruited to this site remained unclear. We therefore asked whether pro-IL-1β is also recruited to speck for caspase-1-dependent cleavage. To monitor the interaction, we co-transfected human full-length (FL) ASC^{FL} and pro-IL-$1β^{FL}$ in HEK293T cells to establish an innovative nano-bioluminescence resonance energy transfer (nanoBRET; NB) reporter assay using NanoLuc (NL) and HaloTag (HL) fusion proteins (Fig. 1 *A* and *B*). In the presence of substrate, NL generates luminescence that excites the nearby HL acceptor through resonance energy transfer, and the nanoBRET ratio was calculated as the acceptor emission divided by the donor emission. Thus, the NB assay provides a proximity-based, live-cell platform well suited for detecting dynamic protein–protein interactions within the inflammasome complex. Heterologous expression of ASC^{FL} in HEK293T cells is sufficient to induce speck formation even in the absence of an activated sensor (5). In addition, HEK293T cells lack gasdermin D (GSDMD), an executioner of pyroptotic cell death; therefore, our NB assay directly probes the recruitment of pro-IL-1β to the speck and excludes confounding effects of caspase-1-dependent pyroptotic cell death. Initially, we determined the optimal tag orientation of donor constructs (N- or C-terminally NL-tagged pro-IL-$1β^{FL}$ and ASC^{FL}), and acceptor constructs (N- or C-terminally HT-tagged human pro-IL-$1β^{FL}$ and ASC^{FL}) (Fig. 1*B* and *SI Appendix*, Fig. S1).

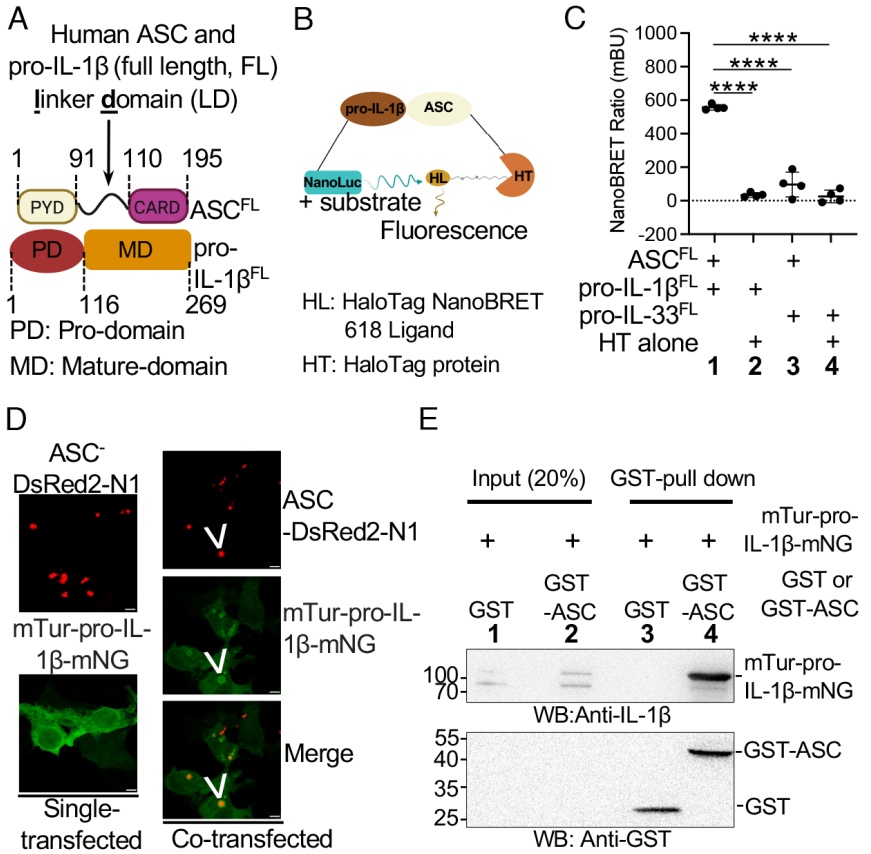

Fig. 1. Direct recruitment of pro-IL-1β to ASC speck enables spatial control of pro-IL-1β maturation. (*A*) Domain organization of human ASC and pro-IL-1β. (*B*) Schematic of NanoBRET assay for ASC/pro-IL-1β interaction. HaloTag (HT)-ASC and pro-IL-1β-NanoLuc (NL) cells were reconstituted in the HEK293T cells. (*C*) ASC/pro-IL-1β interaction assessed by NanoBRET in living HEK293T cells. (*D*) Redistribution and co-localization of pro-IL-1β with ASC in transfected HEK293T cells analyzed by confocal microscopy. *Left* side: HEK293T cells single transfected with either ASC or pro-IL-1β expression construct. *Right* side: HEK293T co-transfected with ASC and pro-IL-1β expression constructs. Representative images are shown. (*E*) Glutathione-S-transferase (GST) pull-down showing interaction between ASC^{FL} and pro-IL-$1β^{FL}$. Data from three independent experiments (*C*), or representative images from three experiments are shown. Data are shown as mean ± SD (n = 4/group). All pairwise comparisons were analyzed using one-way ANOVA with Tukey's post hoc multiple comparison. Brown–Forsythe test was applied to assess homogeneity of variance. (alpha < 0.05). Lane numbers indicate the depicted experimental conditions. ns, not significant; $^{**}P < 0.01$; $^{****}P < 0.0001$. Arrowhead depicts ASC specks or pro-IL-1β. (Scale bar, 5 μm.)

The optimal results were obtained with N-terminally, HT-tagged human ASC, and C-terminally, NL-tagged human pro-IL-1β, which yielded the highest BRET signal.

Toward this, co-transfection of pro-IL-1β^{FL}-NL/HT-ASC^{FL} in living HEK293T cells showed interaction between the two proteins depicted by the high BRET ratios, signifying that the donor (pro-IL-1β^{FL}) and acceptor (ASC^{FL}) are in close proximity (<10 nm) (Fig. 1*C*, lane 1). Our controls included i) HT tags alone co-expressed with NL-tagged pro-cytokines to determine background signal (Fig. 1*C*, lanes 2 and 4); and ii) NL-tagged pro-IL-33 co-expressed with HT-ASC^{FL} as a negative control (Fig. 1*C*, lane 3), as pro-IL-33 is not processed by inflammasomes (17). Distribution of ASC and pro-IL-1β proteins and recruitment of pro-IL-1β to the ASC speck were analyzed by co-localization after co-transfection of plasmids encoding DsRed2-N1-tagged ASC^{WT}, together with pro-IL-1β fused on the N terminus with mTurquoise1 (mTur) and on the C-terminus with mNeonGreen (mNG), creating the mTur-pro-IL-1β-mNG construct (16) (Fig. 1*D*). As expected, HEK293T cells transfected with ASC^{FL} formed specks, whereas pro-IL-1β^{FL} expression was diffuse and evenly distributed in HEK293T cells (Fig. 1*D*, single-transfected, *Left side*). Strikingly, pro-IL-1β^{FL} redistributed in HEK293T cells co-transfected with ASC^{FL} where pro-IL-1β^{FL} reorganized from diffuse distribution to a speck-like appearance, resembling ASC and co-localized with it (Fig. 1*D*, co-transfected, *Right side*). Biochemically, GST pulldown assays were conducted by co-expressing GST-ASC with mTur-pro-IL-1β-mNG (16) in HEK293T cells (Fig. 1*E*). Cell extracts were incubated with GST beads and washed to remove unbound proteins. The bound proteins were eluted and assessed by western blotting. GST-ASC pulled down pro-IL-1β, whereas GST alone did not (Fig. 1*E*, lanes 4 and 3). These findings reveal a previously unrecognized immunoregulatory role of ASC in its ability to recruit pro-IL-1β to the inflammasomes, redefining its function beyond caspase-1 activation.

The Linker Domain of ASC Is Sufficient for pro-IL-1β Binding. We tested the domain requirement for the ASC/pro-IL-1β interaction. Active caspase-1 cleaves pro-IL-1β at D116 ($YVHD_{116}$) sequence to generate the mature p17 fragment responsible for its inflammatory activity. To define the regions of pro-IL-1β domains required for recruitment to ASC, we generated constructs encoding either the pro-domain (IL-1β^{PD}) or the mature domain (IL-1β^{MD}) (Fig. 2*A*). NanoBRET analysis revealed that both IL-1β^{PD} and IL-1β^{MD} exhibited binding to ASC^{FL} (Fig. 2*B*, lanes 2 and 5), indicating that both domains contribute to ASC engagement. ASC contains an N terminus pyrin domain (ASC^{PYD}), a C-terminus CARD (ASC^{CARD}), and a flexible linker domain (ASC^{LD}) in between (18, 19) (Fig. 2*A*). Strikingly, ASC^{LD} alone bound pro-IL-1β^{FL} as robustly as ASC^{FL}, whereas ASC^{PYD} and ASC^{CARD} alone showed minimal binding (Fig. 2*C*, lanes 1 and 3 to 5). Fusion of the PYD to LD (ASC^{PYD+LD}) enhanced pro-IL-1β binding relative to ASC^{PYD} alone, whereas CARD–LD fusion (ASC$^{LD+CARD}$) did not, suggesting that PYD enhances an LD-dependent recruitment mechanism (Fig. 2*C*, lanes 3, 4, 6, and 7). To test the necessity of LD, we engineered ASC variants in which the LD was either replaced by a flexible linker (3× SGSGSG linker, ASC$^{\Delta LD}$) or removed entirely (ASC^{SHORT}). Both constructs showed markedly reduced binding to pro-IL-1β^{FL} comparable to ASC^{WT}, conforming that the LD sequence is required for pro-IL-1β recruitment (Fig. 2*D*, lanes 3 and 4).

As ASC^{LD}, akin to ASC^{FL}, facilitated pro-IL-1β^{FL} binding, we examined macromolecular assemblies generated by these ASC constructs in transfected HEK293T cells by confocal microscopy. As expected, ASC^{FL} assembled into specks with dense cores and emanating filaments (20), while ASC^{PYD} and ASC^{CARD} formed filaments (Fig. 2*E* and *SI Appendix*, Fig. S2*A*). In contrast, ASC^{LD} displayed a granular cytoplasmic distribution with small speckles, whereas ASC^{PYD+LD}, ASC$^{LD+CARD}$, and ASC^{SHORT} formed filaments (Fig. 2*E*). Notably, ASC$^{\Delta LD}$ with the artificial linker, despite lacking pro-IL-1β^{FL} binding capacity, still formed specks comparable to ASC^{FL} (Fig. 2*E*), demonstrating that the molecular composition of LD is not required for speck formation but is essential for pro-IL-1β^{FL} engagement. The alternatively spliced ASCb isoform retains both PYD and CARD and binds pro-caspase-1 with comparable affinity to ASC (21). However, it has only a short linker domain (~3 amino acids), explaining why ASCb is associated with reduced IL-1β maturation (18, 21, 22).

Although pro-IL-1β expression in most myeloid and epithelial cells is NF-κB-dependent, ASC is constitutively expressed, ensuring a preformed adaptor pool for rapid ASC-dependent inflammasome assembly. The ability of ASC^{LD} to form small granular structures and bind pro-IL-1β^{FL} prompted us to ask whether similar ASC^{FL} granules or speckles exist in macrophages as precursor inflammasome platforms. In differentiated THP-1 macrophages with or without LPS priming, ASC immunostaining (AL177; Adipogen) revealed granular and speckled cytoplasmic distribution, which consolidated into distinct specks upon inflammasome activation (Fig. 2 *F*, *Top, Middle, and Bottom* panel). To specifically examine whether ASC^{LD} is accessible in the ASC speck, we raised an anti-LD antibody in-house (*SI Appendix*, Fig. S2*B*). Immunofluorescence (IF) with this antibody revealed a comparable granular/speckled ASC pattern as observed with the commercial antibody in THP-1 cells (Fig. 2 *G*, *Top, Middle, and Bottom* panel). Similar patterns were also observed in untreated or LPS-primed primary human peripheral blood mononuclear cells (PBMCs) (*SI Appendix*, Fig. S2 *C–E*), confirming that the LD region is exposed and accessible within native specks.

To determine whether ASC granules or speckles associate with pro-IL-1β, we performed IF microscopy following LPS priming or at 60 min post-NLRP3 inflammasome activation, using antibodies specific for either the mature or the pro-domain of pro-IL-1β (*SI Appendix*, Fig. S2 *F–L*). Under LPS-primed conditions, ASC granules or speckles in the cytosol appeared partially co-localized with cytosolic pro-IL-1β. In contrast, activation with nigericin induced robust ASC speck formation, accompanied by a reduction of cytosolic IL-1β signal, consistent with pro-IL-1β processing and release of mature pro-IL-1β within this time frame (16). Together, these findings identify ASC^{LD} as a key structural element mediating pro-IL-1β recruitment. Our data further suggest that ASC^{LD} positive granules/speckles could represent early or pre-assembly inflammasome platforms that have already recruited pro-IL-1β for efficient cytokine processing upon activation.

Structural and Molecular Determinants of pro-IL-1β for ASC Binding. Although both pro- and mature domains of IL-1β can interact with ASC (Fig. 2*B*), the IL-1β^{PD} signals exhibited substantial variability whereas IL-1β^{MD} produced consistently robust NanoBRET signals, surpassing even those of pro-IL-1β^{FL}. We thus decided to map the interaction of IL-1β^{MD} with ASC. Guided by AlphaFold (23, 24), and the X-ray crystal structure of human IL-1β (PDB:9ILB) (25), we systematically mutated surface-exposed, charged residues within IL-1β^{MD} and assessed ASC engagement using the NanoBRET assay (Fig. 3*A*). A discrete set of IL-1β^{MD} domain mutants (R127E, D128A, K143E, K190E/K193E, and K204E) significantly disrupted ASC binding (Fig. 3 *B* and *C* and *SI Appendix*, Fig. S3).

To determine the functional significance of this interface, we reconstituted *IL1B*$^{-/-}$ THP-1 cells with individual IL-1β^{MD}

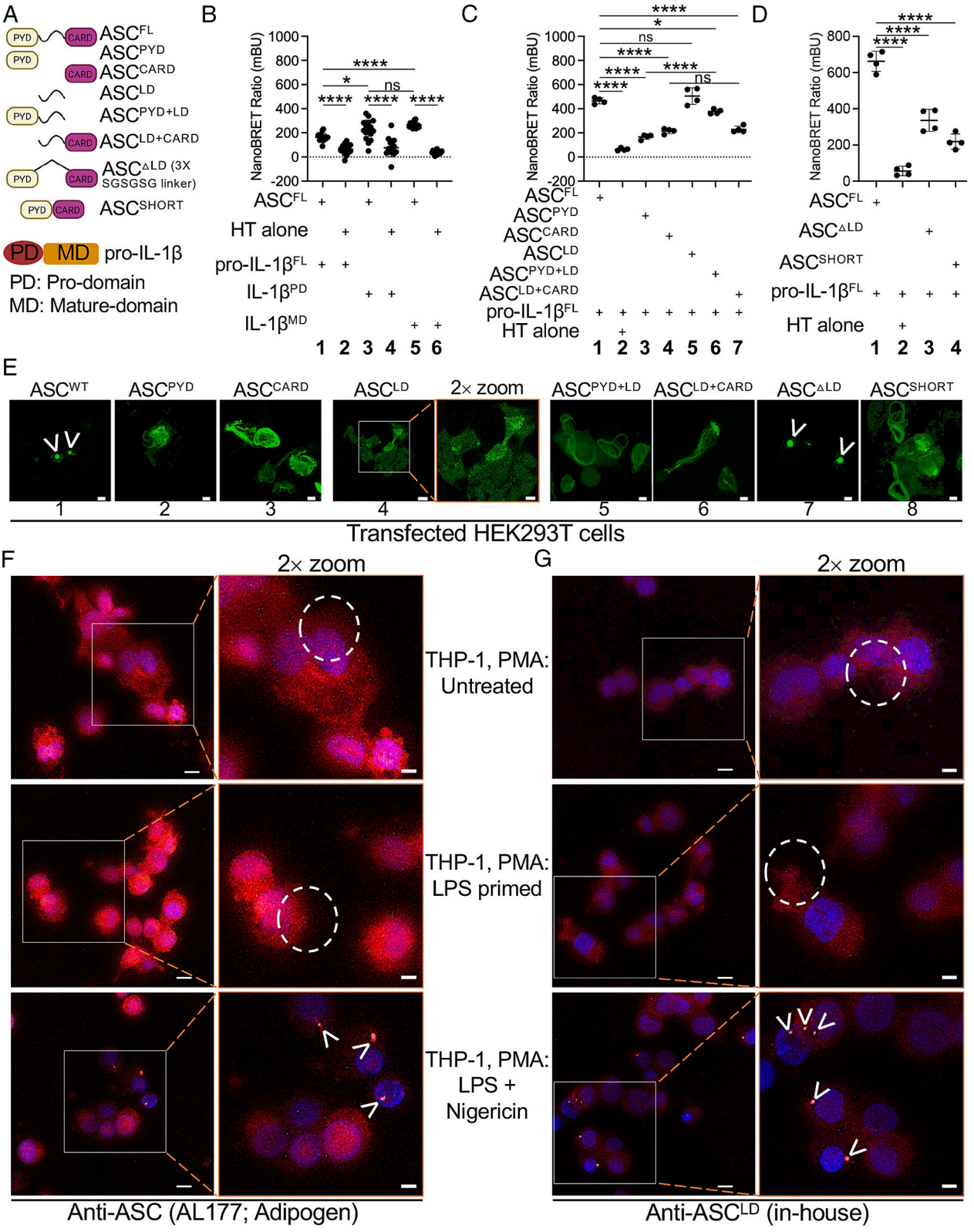

Fig. 2. Molecular determinants governing ASC/pro-IL-1β interactions. (*A*) Domain organization of full-length ASC and constructs used in the study. (*B*) Requirement of pro-IL-1β pro- and mature domains for ASC binding, assessed by NanoBRET assay. (*C*) Binding of pro-IL-1β to ASC^{FL} and individual ASC domains measured by nanoBRET assay. (*D*) Comparison of pro-IL-1β binding to ASC^{FL}, ASC$^{\Delta LD}$ and ASC^{SHORT} by nanoBRET assay. (*E*) Macromolecular assemblies formed by ASC domain constructs described in (*A*), visualized by confocal microscopy following paraformaldehyde fixation and HT immunolabeling of transfected HEK293T cells. (*F*) Detection of endogenous ASC N terminus domain using a commercial ASC antibody (AL177; Adipogen) in THP-1 cells (untreated, LPS primed, or LPS + Nigericin treated) analyzed by confocal microscopy. (*G*) Detection of endogenous ASC linker domain using in-house developed ASC antibody in THP-1 cells under same condition as in (*F*) analyzed by confocal microscopy. Data represent three independent experiments (*B*–*D*), or representative images from two experiments (*E*–*G*). Data are shown as mean ± SD (n = 16/group, *B*; n = 4/group, *C* and *D*). All pairwise comparisons were analyzed using one-way ANOVA with Tukey's post hoc multiple comparison. Brown–Forsythe test was applied to assess homogeneity of variance. Lane numbers indicate the depicted experimental conditions. (alpha < 0.05). ns, not significant; *P < 0.05; ****P < 0.0001. [Scale bar, 5 μm (E_1–E_3 and E_5–E_8); 20 μm (E4; 2× zoom = 10 μm); 10 μm (*F* and *G*; 2× zoom = 5 μm).] Arrowheads indicate specks. Dotted circle highlights granular or speckle-like ASC distribution.

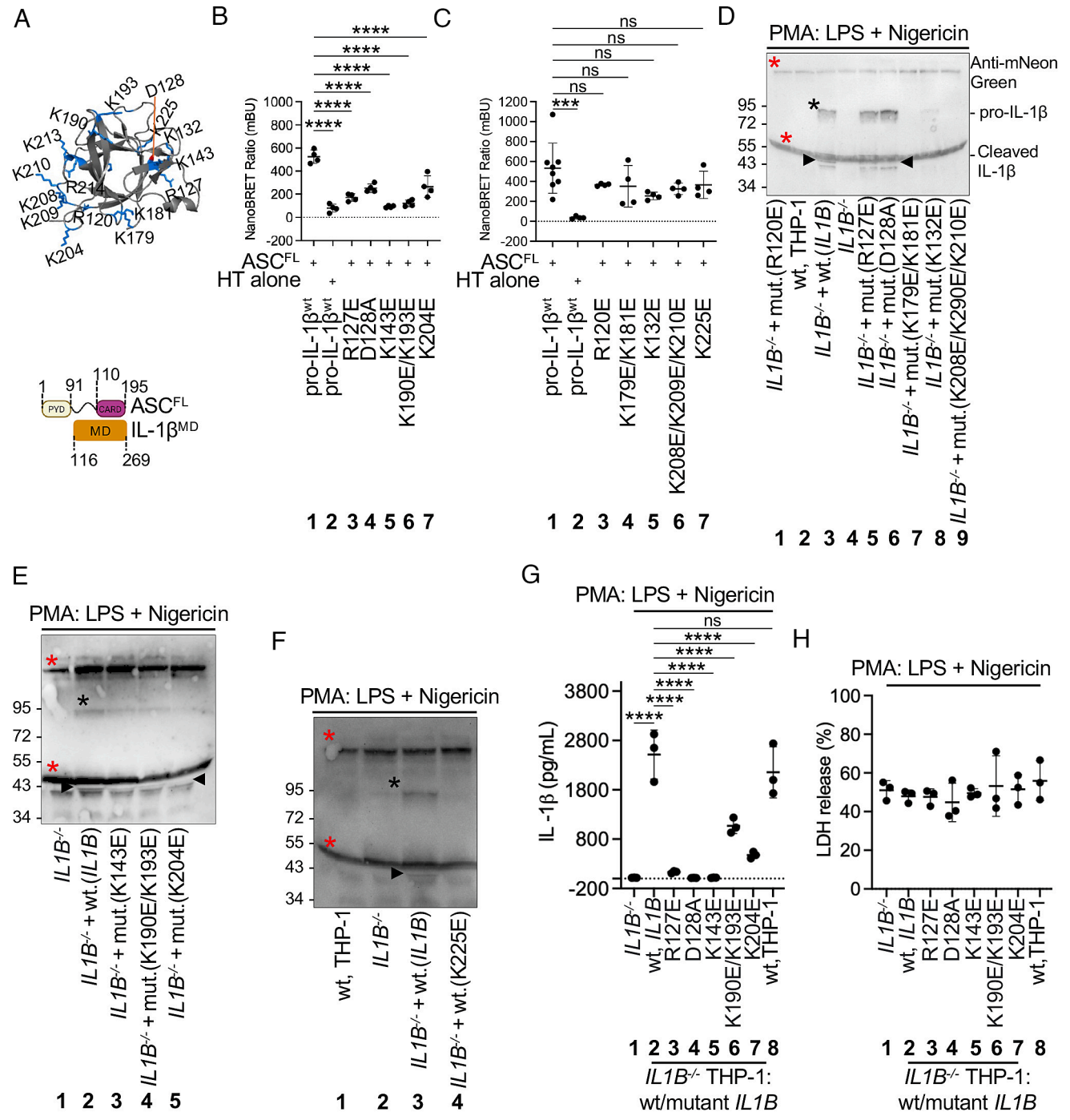

Fig. 3. Structure-guided mapping of pro-IL-1β binding determinants required for ASC binding. (*A*) AlphaFold model of human IL-1β (mature domain) generated using the X-ray crystal structure (PDB:9ILB) as template. (*B* and *C*) NanoBRET analysis of ASC/pro-IL-1β interactions using mature domain mutants in the HEK293T cells. (*D–F*) Caspase-1-dependent cleavage of pro-IL-1β mutants reconstituted in *IL1B*$^{-/-}$ THP-1 cells following NLRP3 activation, assessed by immunoblot. Cleavage was analyzed by immunoblotting with an anti-mNG specific antibody. The mature domain–mNG fusion migrated at ~44.55 kDa (arrowhead). Black asterisk depicts full-length pro-IL-1β labeled with N-terminal mTur and C-terminal with mNG (Tur-pIL-1β-NG). The red asterisk marks non-specific band. (*G*) Secreted mature-IL-1β from reconstituted *IL1B*$^{-/-}$ THP-1 cells expressing wild-type (WT) or mutant pro-IL-1β during NLRP3 activation. (*H*) Cell death in reconstituted *IL1B*$^{-/-}$ THP-1 cells expressing WT or mutant pro-IL-1β during NLRP3 activation. Data represent two independent experiments and are shown as mean ± SD (*B* and *C*, *n* = 3/group; *G*, *n* = 3/group). All pairwise comparisons were analyzed using one-way ANOVA with Tukey's post hoc multiple comparison. Brown–Forsythe test was applied to assess homogeneity of variance. (alpha < 0.05). Lane numbers indicate the depicted experimental conditions. ns, not significant; ***P < 0.001; ****P < 0.0001.

variants. Importantly, all IL-1β^{MD} mutants that impaired ASC binding in NanoBRET assays showed a marked decrease in IL-1β processing upon inflammasome activation when reconstituted in *IL1B*$^{-/-}$ THP-1 cells (Fig. 3 *D–G*). In contrast, pyroptosis, assessed by lactate dehydrogenase (LDH) release, was comparable to WT reconstituted cells (Fig. 3*H*). These findings indicate that ASC recruitment to IL-1β specifically governs cytokine processing without perturbing pyroptotic execution. A second category of mutants (R120E, K179E/K181E, K132E, K208E/K209E/K210E, K225E), while showing unperturbed interaction with ASC in nanoBRET assay, could not be evaluated functionally because they exhibited low or undetectable expression in reconstituted THP-1 cells (Fig. 3 *D* and *F*). This expression limitation may reflect instability or misfolding of certain IL-1β variants in the reconstituted

THP-1 system rather than lack of biological relevance. Notably, the D128A substitution (D129 in mouse IL-1β) (26) previously shown to disrupt an intramolecular electrostatic interaction with K132 (K133 in mouse IL-1β) (26) also impaired ASC binding shown by NanoBRET (Fig. 3*B*, lane 4), pro-IL-1β cleavage when reconstituted into *IL1B*$^{-/-}$ THP-1 cells (Fig. 3*D*, lane 6), and IL-1β secretion (Fig. 3*G*, lane 4). Together, these data identify the IL-1β mature domain region as an important determinant for recruitment to ASC and establish the ASC/IL-1β interface as a key regulatory checkpoint that ensures efficient IL-1β maturation without limiting beneficial pyroptotic cell death response.

ASC^{LD} Defines a Discrete, Noncanonical Binding Interface Required for pro-IL-1β Recruitment. ASC speck formation proceeds through polymerization of N terminus ASC^{PYD} into filaments, followed by ASC^{CARD} driven condensation into a micron-sized structure known as ASC speck (20, 27). Mutations that disrupt ASC oligomerization (ASC$^{PYDmut.}$) or filament cross-linking (ASC$^{CARDmut.}$) are known to impair speck formation and consequently impede pro-IL-1β maturation (20). While these structured domains are well characterized, how the intrinsically flexible ASC^{LD} (22) directly contributes to pro-IL-1β processing remained undefined (18, 19). To address this question, we systematically substituted proline and glycine residues in ASC^{LD} with alanine residues (G92A, G94A, G99A, P97A, P104A, P110A) and assessed pro-IL-1β^{FL} binding using the NanoBRET assay (Fig. 4*A* and *SI Appendix*, Fig. S4*A*). We also mutated the K109 residue within this region, whose SUMOylation by ZBTB16 (zinc-finger and BTB domain-containing protein 16) was shown to enhance ASC oligomerization (28) (Fig. 4*B*). Among these ASC^{LD} mutants, only P97A and P104A significantly disrupted binding with pro-IL-1β (Fig. 4*A*, lanes 5 and 7). To

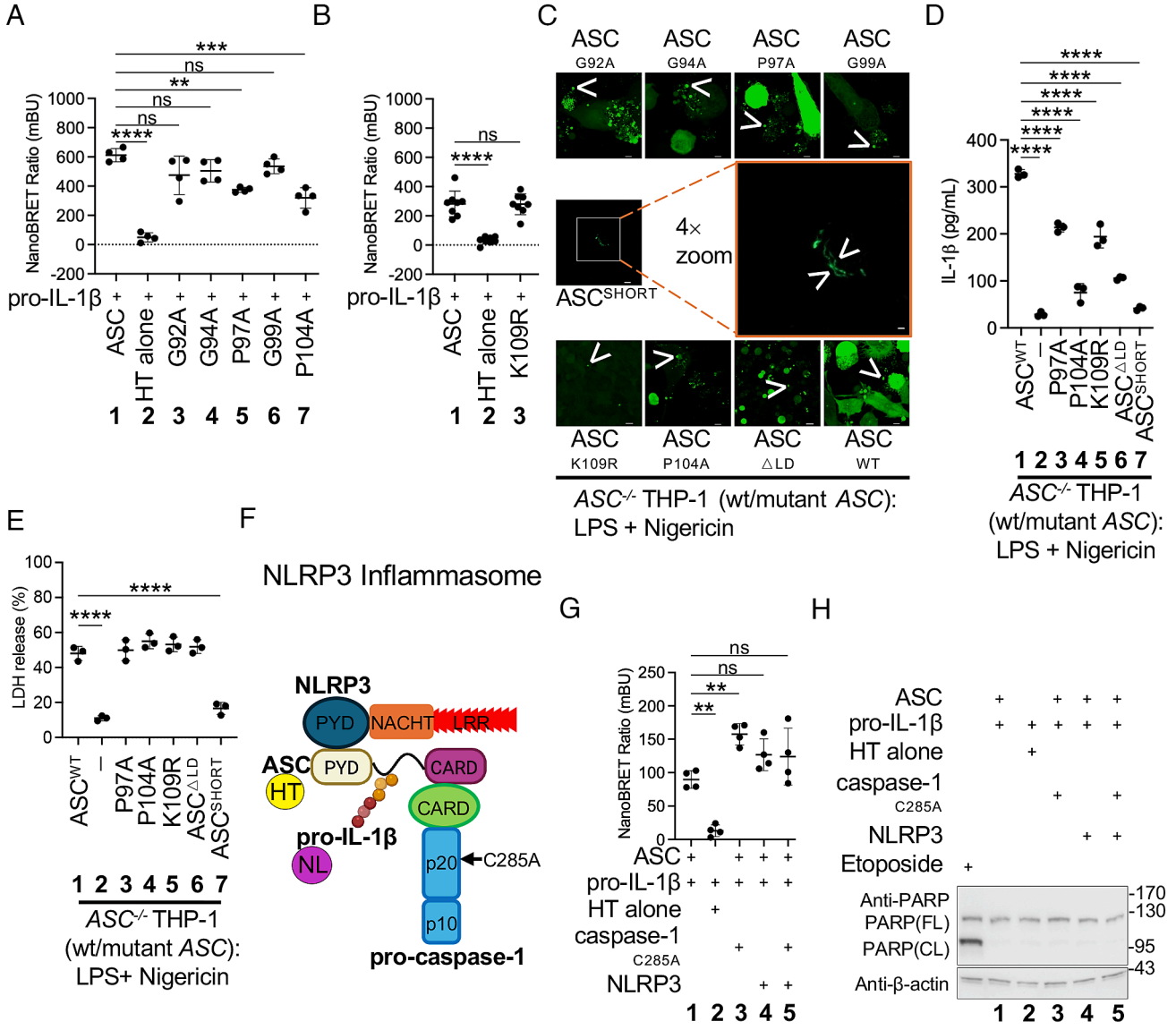

Fig. 4. The ASC interlinker domain specifies a discrete binding surface for pro-IL-1β recruitment. (*A* and *B*) NanoBRET analysis of interaction between ASC (WT or interlinker domain mutants) and pro-IL-1β in HEK293T cells. (*C*) ASC speck formation in *ASC*$^{-/-}$ THP-1 cells reconstituted with WT or mutant ASC following NLRP3 activation. (*D*) Secreted mature-IL-1β from reconstituted *ASC*$^{-/-}$ THP-1 cells following NLRP3 inflammasome activation. (*E*) Cell death in reconstituted *ASC*$^{-/-}$ THP-1 following NLRP3 inflammasome activation. (*F*) Schematic of the NLRP3 inflammasome reconstituted in HEK293T cells. (*G*) NanoBRET assessment of LD domain accessibility under canonical PYD–PYD and CARD–CARD interactions. (*H*) Cell death analysis in HEK293T cells reconstituted NLRP3 inflammasome. Images or data from two independent experiments (*A*, *B*, *D*, *E*, and *G*) are shown. Data are shown as mean ± SD (*A* and *G*, *n* = 4/group; *B*, 8/group; *D* and *E*, 3/group). All pairwise comparisons were analyzed using one-way ANOVA with Tukey's post hoc multiple comparison. Brown–Forsythe test was applied to assess homogeneity of variance. (alpha < 0.05). Lane numbers indicate the depicted experimental conditions. ns, not significant; ***P* < 0.01; ****P* < 0.001; *****P* < 0.0001. [Scale bar, 5 μm (4× zoom = 1.25 μm).] Arrowheads indicate specks or filaments.

test the functional consequence of these disruptive mutations, *ASC*$^{-/-}$ THP-1 cells were reconstituted with WT or LD-mutant ASC. Despite forming normal ASC speck (Fig. 4*C*), P97A and P104A significantly decreased mature IL-1β production following LPS priming and NLRP3 activation (Fig. 4*D*), without affecting pyroptosis as measured by LDH release (Fig. 4*E*). Although ASC SUMOylation at K109 should promote ASC oligomerization, the preserved ASC/pro-IL-1β interaction in the SUMO-deficient ASC^{K109R} mutant suggests that SUMOylation is not required for pro-IL-1β binding (Fig. 4 *B-E*). Removing the entire linker domain (ASC^{SHORT}) eliminated both speck assembly (formed filaments) and pro-IL-1β maturation, whereas replacing the entire LD with a flexible 3× SGSGSG linker (ASC$^{\Delta LD}$) preserved speck assembly but abolished pro-IL-1β^{FL} binding and reduced IL-1β maturation (Figs. 2 *D* and *E* and 4 *C* and *D*). Thus, ASC^{LD} is specifically required for both ASC oligomerization and cytokine processing but is dispensable for pyroptosis. Because pro-IL-1β engages ASC^{LD}, we next tested whether this interaction perturb canonical PYD–PYD or CARD–CARD interfaces within the inflammasomes. HEK293T cells lack endogenous caspase-1 and GSDMD. Reconstitution of the NLRP3 inflammasome in HEK293T confirmed that ASC^{LD}/pro-IL-1β binding measured by NanoBRET remained intact even in the presence of NLRP3^{PYD}–ASC^{PYD} and ASC^{CARD}–pro-caspase-1^{CARD} interactions (Fig. 4 *F* and *G*). The catalytically dead caspase-1 (C285A) was used in the reconstitution to prevent pyroptotic membrane rupture. Although ASC has been reported to nucleate pro-caspase-8 filaments at inflammasomes thereby promoting apoptotic cell death (29, 30), lack of apoptotic protease-mediated PARP cleavage confirmed that our reconstituted NLRP3/ASC/caspase-1^{C285A}/pro-IL-1β system is non-lytic (Fig. 4*H*). Thus, the ASC^{LD}/pro-IL-1β recruitment occurs in intact, viable cells, not driven by membrane lysis. Together, these data demonstrate that the ASC linker domain is a distinct, accessible, and noncanonical surface within the ASC speck for pro-IL-1β recruitment, does not interfere with inflammasome assembly, and mediates a key regulatory checkpoint that governs IL-1β maturation without limiting beneficial pyroptotic death.

ASC^{LD}-Derived Peptide Blocks pro-IL-1β Processing in Primary Macrophages and THP-1 Cells. Since ASC^{LD} is sufficient for pro-IL-1β interaction, likely both before and after ASC speck formation, we synthesized the ASC^{LD} peptide fused at its C-terminal end to the antennapedia sequence for intracellular delivery (31) (Peptide^{LD}), as well as a control peptide derived from the C-terminal end of ASC^{CARD} (Peptide^{CTR}) (Fig. 5*A*). We isolated monocytes from human PBMCs of a healthy volunteer and generated monocyte-derived macrophages (MDMs) (Fig. 5*A*). Peptide^{LD} pre-treated to human MDMs prior to LPS priming and NLRP3 activation with nigericin significantly reduced secreted mature-IL-1β in supernatants as quantified by Enzyme-linked immunosorbent assay (ELISA) (Fig. 5*B*, lane 4), while pyroptotic cell death remained unaffected, as indicated by comparable LDH release (Fig. 5*C*, lane 4). By contrast, Peptide^{CTR} had no observable effect and was similar to vehicle-treated + LPS + nigericin stimulated condition, supporting a specific requirement for LD in pro-IL-1β recruitment and maturation (Fig. 5 *B* and *C*). Similar to THP-1 cells, ASC^{LD} is exposed within endogenous ASC specks formed in MDMs, shown by IF experiments at basal, LPS-primed, and LPS + nigericin conditions using either the in-house LD specific antibody or the commercial ASC antibody (Fig. 5 *D–F* and *SI Appendix,* Fig. S5 *A–D*).

Peptide-inhibition studies in THP-1 cells showed similar results with Peptide^{LD} decreasing mature IL-1β without changes in LDH release (Fig. 5 *G* and *H* and *SI Appendix,* Fig. S5*E*), confirming that LD domain-mediated recruitment is conserved across endogenous inflammasome platforms in both primary and immortalized cells. The reduction in IL-1β maturation was not attributable to impaired priming as Peptide^{LD} did not alter pro-IL-1β or NLRP3 expression under either primed or activated condition (Fig. 5*I*). Caspase-1 activation was also comparable, as evidenced by the presence of the cleaved p20 subunit (Fig. 5*I*), indicating that reduction in IL-1β maturation resulted from impairment in pro-IL-1β recruitment rather than from impaired inflammasome assembly or signaling. Together, these results reveal that peptide based on ASC^{LD} can interfere with the recruitment and positioning of pro-IL-1β for caspase-1-dependent maturation, which provides a proof of principle for targeting the ASC/pro-IL-1β interaction against IL-1β-driven inflammation.

ASC^{LD} Targeting Preserves ASC Speck Assembly While Impairing pro-IL-1β Recruitment. As ASC oligomerization is necessary for both speck formation and pro-IL-1β maturation, and Peptide^{LD} prevented pro-IL-1β maturation, we asked whether it also perturbs ASC speck formation. To test this directly, we transfected untreated or peptide-treated HEK293T cells with an ASC-mTurquoise construct and visualized speck formation by fluorescence microscopy. ASC speck formed robustly in all conditions (Fig. 6*A* and *SI Appendix,* Fig. S6*A*), and the LD epitope remained exposed on these specks, as detected by an ASC^{LD}-specific antibody (*SI Appendix,* Fig. S6*B*). These data indicate that the LD is accessible on the specks and its blockade does not impair speck assembly.

We examined the functional consequence of peptide treatment on pro-IL-1β in HEK293T cells co-expressing ASC. Under vehicle or Peptide^{CTR} treated conditions, pro-IL-1β redistributed from a diffuse cytosolic pattern to speck-like puncta that co-localized with ASC, indicating recruitment to specks (Fig. 6*B* and *SI Appendix,* Fig. S6*C*). In contrast, Peptide^{LD} treatment reduced the relocalization despite the formation of normal ASC specks, with pro-IL-1β remaining diffuse in most cells shown by quantification (Fig. 6*B* and *SI Appendix,* Fig. S6*C*). These results demonstrate that Peptide^{LD} treatment uncoupled pro-IL-1β docking from speck assembly. Together, these findings support a model in which ASC^{LD} not only required for ASC speck formation but also is exposed on speck for pro-IL-1β recruitment. By selectively perturbing pro-IL-1β recruitment, Peptide^{LD} inhibits pro-IL-1β processing without compromising inflammasome assembly. Our data identify an intracellular regulatory checkpoint for pro-IL-1β recruitment and reveals a therapeutically accessible mechanism for selectively modulating pro-IL-1β maturation.

ASC^{LD} Is Required for MSU- and ATP-Induced Inflammation In Vivo. To define the in vivo role of the ASC linker domain in pro-cytokine recruitment, and inflammasome-dependent IL-1β maturation, we evaluated two established mouse models of NLRP3-dependent peritonitis: MSU-induced peritonitis (32) and LPS + ATP-induced peritonitis (33) (Fig. 7). These models are NLRP3-dependent, but they differ in the upstream signaling mechanism. MSU, a damage-associated molecular pattern (DAMP), provides both priming and activating signals and mimics sterile inflammation as seen in gouty arthritis inflammation (34), in which the early infiltrating immune cells are primarily neutrophils during the onset of peritonitis, and the number of infiltrating neutrophils in the peritoneal cavity correlates with the extent of inflammasome activation (35, 36). The LPS + ATP model utilized two sequential signaling steps, conferred by a bacterial pathogen-associated molecular pattern

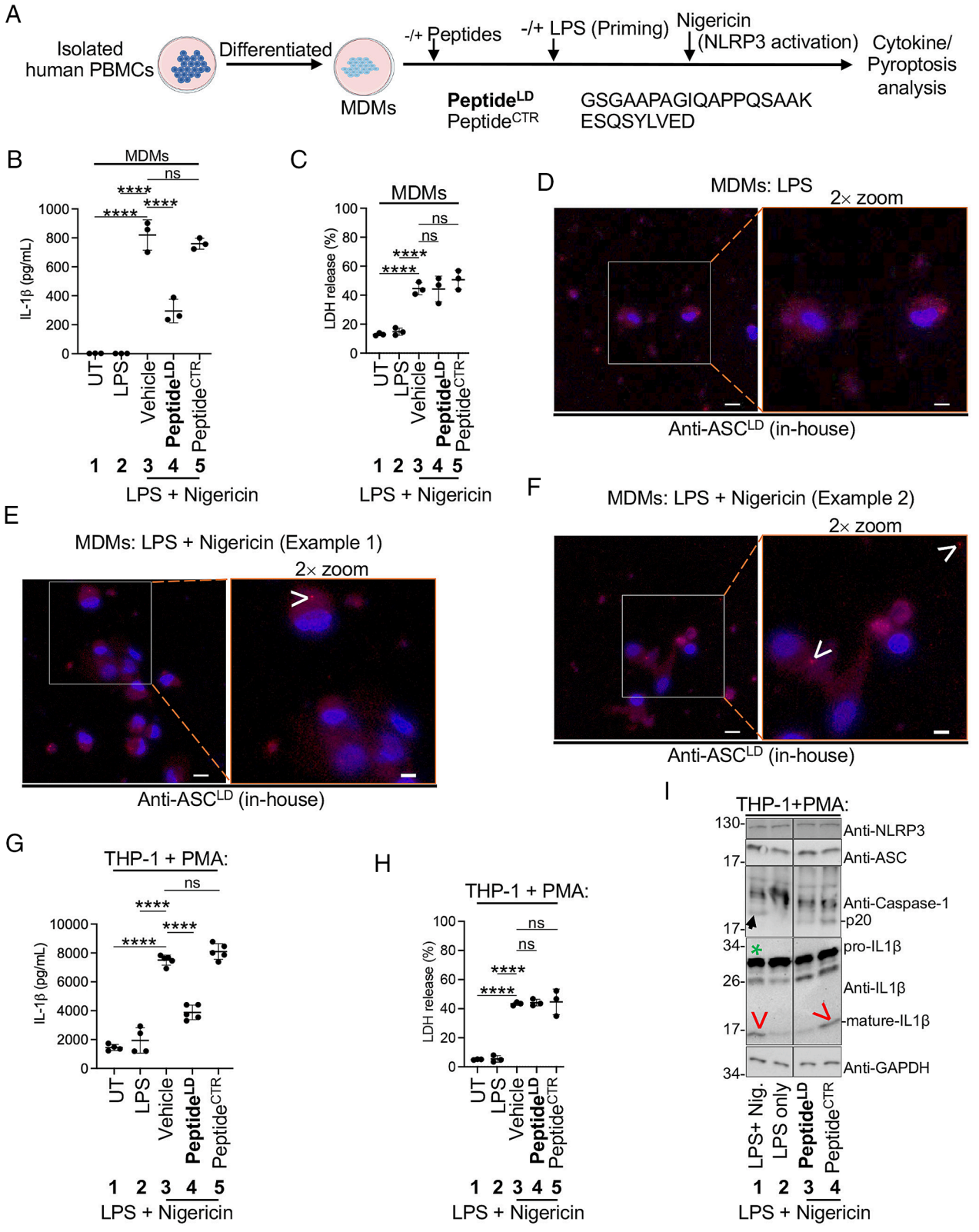

Fig. 5. ASC^{LD} is required for pro-IL-1β processing primary macrophages and in THP-1 cells. (*A*) Schematic of peptide-inhibition studies in human MDMs. The sequences of the linker-domain peptide (Peptide^{LD}) and the control peptide (Peptide^{CTR}) are shown. (*B* and *C*) IL-1β secretion (*B*) and cell death (*C*) in human MDMs untreated or pretreated with linker-domain or control peptide, prior to LPS priming and nigericin stimulation. (*D–F*) ASC speck formation and LD accessibility in human MDMs, detected using a custom ASC^{LD} antibody. Panel D shows LPS-primed cells, and panels *E* and *F* show representative examples following LPS priming and nigericin activation. White arrowhead depicts ASC specks detected by ASC^{LD}-specific antibody. (*G* and *H*) IL-1β secretion (*G*) and cell death (*H*) in THP-1 cells untreated or pre-treated with linker-domain or control peptide, prior to LPS priming and NLRP3 activation with nigericin. (*I*) Western blotting analysis of inflammasome components in THP-1 cells following peptide treatment, LPS priming, and nigericin stimulation. Black arrowhead, cleaved caspase-1 band (p20); green asterisk, pro-IL-1β (34 kDa); red arrowhead, cleaved IL-1β (17 kDa). Data represent three independent experiments and are shown as mean ± SD (n = 3 to 5/group). All pairwise comparisons were analyzed using one-way ANOVA with Tukey's post hoc multiple comparison. Brown–Forsythe test was applied to assess homogeneity of variance. (alpha < 0.05). Lane numbers indicate the depicted treatment conditions. ns, not significant; ****P < 0.0001. [Scale bar, 10 μm (*D–F*; 2× zoom = 5 μm).]

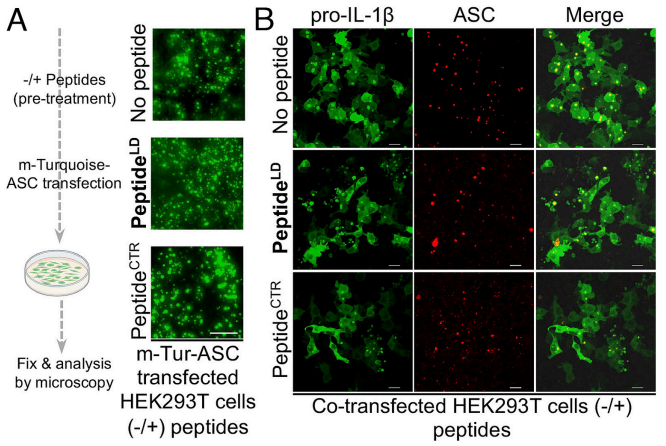

Fig. 6. ASC^{LD} targeting preserves ASC speck assembly while impairing pro-IL-1β recruitment. (*A*) Confocal imaging of ASC speck formation in HEK293T cells pretreated for 2 h with linker-domain (Peptide^{LD}) or control peptide (Peptide^{CTR}) prior to ASC-mTurquoise transfection. (*B*) Confocal imaging of pro-IL-1β (green) and ASC (red signal) in transfected HEK293T cells pretreated for 2 h with indicated peptides. Representative images showing redistribution of pro-IL-1β signals to ASC specks in untreated cells or in cells treated with either Peptide^{LD} or Peptide^{CTR} as depicted. (Scale bar, (*A*) 100 μm; (*B*) 20 μm.)

(PAMP) (such as LPS) for priming and a host-derived signal (ATP) for NLRP3 inflammasome activation, generating a broader and tightly regulated inflammatory response.

Wildtype C57BL/6 mice were pre-treated with vehicle, Peptide^{CTR}, or Peptide^{LD} prior to inflammasome activation (Fig. 7*A*). As expected, MSU challenge induced robust peritoneal neutrophil infiltration (Ly-6G^{+ve} Ly-6B.2^{+ve} cells) and IL-1β production in vehicle- or Peptide^{CTR}-treated mice (Fig. 7 *B–D*). In contrast, Peptide^{LD} significantly reduced both IL-1β levels and neutrophil recruitment in the peritoneal lavage (Fig. 7 *B–D*). In the LPS + ATP model, pretreatment with Peptide^{LD} significantly decreased IL-1β production in the plasma (Fig. 7 *E* and *F*). Unexpectedly, Peptide^{LD} showed selective activity in the LPS + ATP model as it reduced systemic (plasma) IL-1β but failed to suppress cytokine production in the peritoneal cavity (Fig. 7 *E* and *G*). This differential activity likely reflects context-dependent peptide stability, biodistribution, and cellular uptake across an inflammatory environment. In the MSU model, inflammation occurs locally within a sterile peritoneal milieu dominated by resident peritoneal macrophages and early neutrophil influx. Under these conditions, Peptide^{LD} likely remained stable and was sufficiently concentrated to block the ASC/pro-IL-1β interaction. In contrast, the LPS + ATP model involves systemic priming, enhanced vascular permeability, and robust ATP-driven activation, a condition that may enhance proteolytic degradation or dilute local Peptide^{LD} concentration, thereby limiting its inhibitory capacity. Together, these findings demonstrate that the ASC linker domain is indispensable for efficient pro-IL-1β maturation in vivo. Disrupting ASC/pro-IL-1β interface using the cell-penetrating peptide attenuates inflammation across mechanistically distinct NLRP3-dependent contexts, highlighting ASC^{LD} as a regulatory node that couples pro-IL-1β recruitment to downstream inflammatory response.

Discussion

Inflammasome protects host from both infectious and sterile injuries by coupling caspase-1 activation to IL-1β maturation, yet the molecular mechanism that positions pro-IL-1β for cleavage has remained undefined. Here, we identify the ASC linker domain, a flexible, previously uncharacterized region between the PYD and CARD as a dedicated docking interface that recruits pro-IL-1β to the ASC speck. The present findings establish a conceptual shift by identifying ASC as not only a signaling scaffold for caspase-1 activation but also a spatial organizer that concentrates the pro-IL-1β substrate at the site of processing (*SI Appendix,* Fig. S8).

Using multiple orthogonal approaches, including NanoBRET, cellular imaging, targeted mutagenesis, synthetic peptide inhibition, and in vivo perturbation, we show that ASC^{LD} provides a noncanonical binding surface that remains exposed within the native, endogenously assembled speck. The IL-1β mature domain region encodes residues necessary for ASC engagement, forming a discrete interface that is essential for pro-IL-1β processing but dispensable for pyroptosis. These findings define ASC/pro-IL-1β recruitment as a regulatory checkpoint that modulates IL-1β output independently of pyroptosis, permitting selective control of inflammatory potency without compromising host-protective pyroptosis.

An intriguing implication of our findings is that even cleaved, mature IL-1β retains the capacity to interact with ASC, raising the question of how mature IL-1β is ultimately released from cells. This interpretation is particularly interesting in light of observations by Singer et al., who reported that mature-IL-1β is generated following the association of pro-IL-1β and caspase-1 with the plasma membrane during secretion (37). Since the initial description of inflammasomes, subsequent studies have identified mechanistic aspects of IL-1β maturation and release (8, 38–40). More recent work has shown that mature-IL-1β is directed toward plasma membrane projections or vesicular structures and can exit the cell through both gasdermin D (GSDMD)-dependent rapid pathways and GSDMD-independent slower routes, irrespective of ultimate cell fate (41). Based on these findings, we propose that retention of mature IL-1β on ASC might serve to transiently sequester the cytokine until appropriate permeabilization occurs, either through GSDMD pore formation or increased membrane tension, thereby limiting premature intracellular diffusion, aberrant signaling, or proteolytic degradation.

Our data support a model in which the ASC/pro-IL-1β interaction is not dependent on the ASC oligomerization state. That is, small ASC speckles or granules in the cytosol and the large ASC speck both represent pro-IL-1β recruitment-competent forms. Thus, even before inflammasome activation, pro-IL-1β is already associated with ASC, at least partly, such that as soon as caspase-1 gets recruited and activated at the ASC speck, cleavage of pro-IL-1β by caspase-1 can occur. This intricate control explains how IL-1β processing is both rapid and insulated from fluctuations in downstream pyroptotic execution. Because of the intrinsic flexibility of the ASC linker domain, the recent cryo-EM structure did not resolve density corresponding to this region (22). Our systematic alanine-scanning analysis across this flexible stretch unveiled a continuous functional surface, with P97 and P104 emerging as key determinants of pro-IL-1β engagement. Given the short, unstructured nature of the LD, it is likely that these residues, together with the surrounding linker aid in stabilizing the docking interface for pro-IL-1β that operates independently of canonical PYD–PYD or CARD–CARD interactions. Consistent with an LD-specific mechanism, ASC SUMOylation at K109, previously linked to ASC oligomerization (28), was dispensable for pro-IL-1β binding, indicating that pro-IL-1β recruitment does not rely on global effects of ASC assembly. These studies further warrant detailed structural studies to elucidate the extent of interaction interface in ASC/pro-IL-1β.

The importance of ASC^{LD}-mediated recruitment is underscored by the striking in vivo requirement for this interface. ASC^{LD}-targeting peptides markedly reduced IL-1β production and

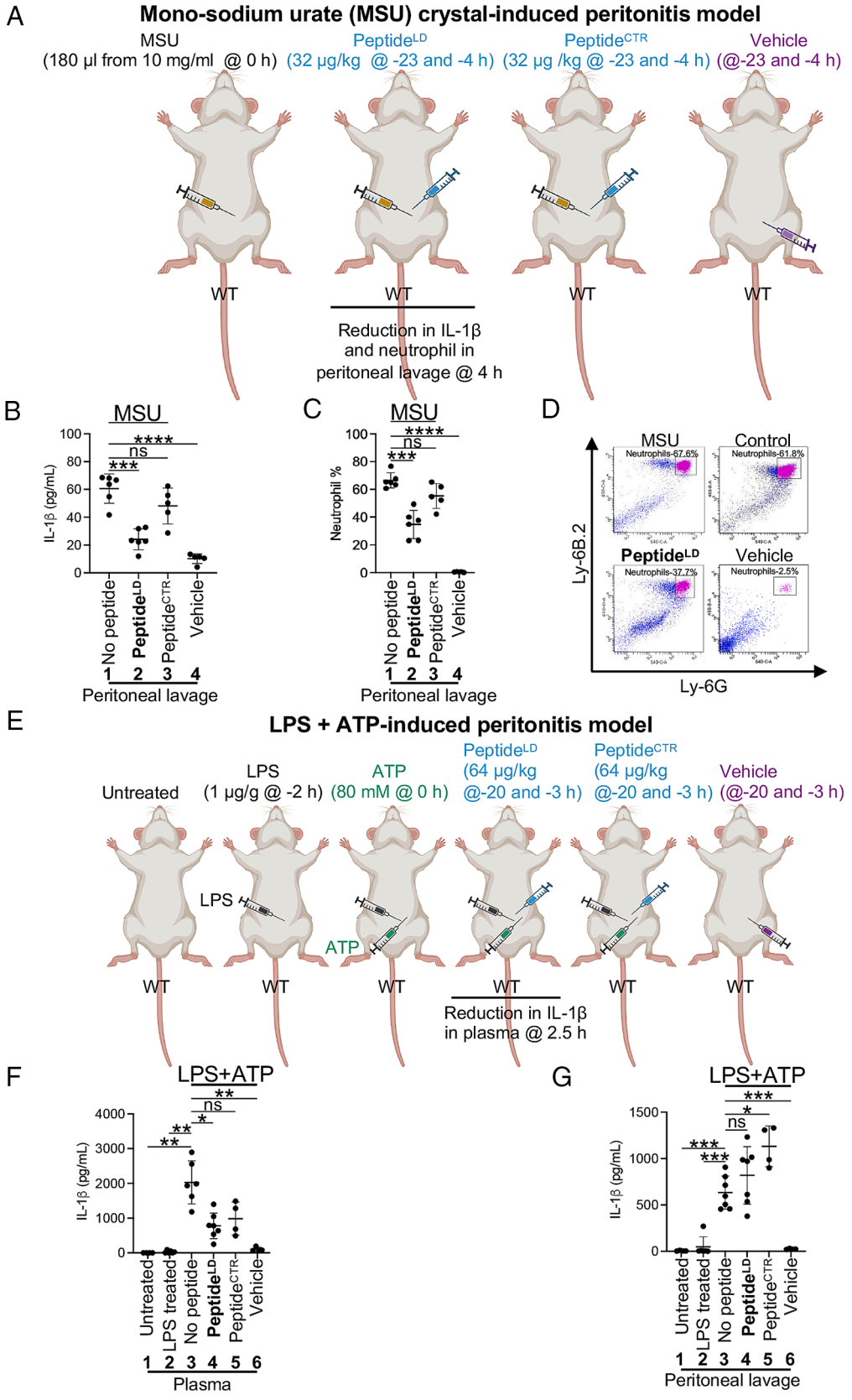

Fig. 7. ASC^{LD} is required for MSU- and ATP-induced inflammation in vivo. (*A–D*) MSU-induced peritonitis model. (*A*) Schematics with indicated dosing and experimental timeline. (*B*) IL-1β levels in peritoneal lavage following peptide treatment. (*C* and *D*) Neutrophil recruitment in peritoneal lavage and quantification, assessed by flow cytometric analysis of Ly6G^{+}/Ly6B.2^{+} neutrophils in peritoneal lavage (*C*), and corresponding quantification (*D*). (*E–G*) LPS + ATP-induced peritonitis model. (*E*) Schematics with indicated dosing and experimental timeline. (*F* and *G*) IL-1β levels in plasma (*F*) and peritoneal lavage (*G*). Data are shown as mean ± SD (n = 4 to 7/group). For pairwise comparisons between each group and +ve control (No peptide + NLRP3 activation condition), data were analyzed using one-way ANOVA with Welch's correction. Brown–Forsythe test was applied to assess homogeneity of variance. Post hoc comparison adjustment was performed using Dunnett's T3 (alpha < 0.05). Lane numbers indicate the depicted treatment conditions. ns, not significant; *P < 0.05; **P < 0.01; ***P < 0.001; ****P < 0.0001.

neutrophil influx in two NLRP3-dependent peritonitis models, highlighting the importance of this interaction in inflammatory signaling. Although linker-domain peptide showed consistent activity across models, we did observe context-dependent inhibition, suppressing systemic IL-1β in LPS + ATP challenge but not local peritoneal production. This differential behavior likely reflects variations in peptide stability, proteolytic degradation, and tissue distribution under sterile (MSU) versus endotoxin-primed inflammatory conditions, rather than a fundamental mechanistic difference in LD dependency.

Importantly, the ability to attenuate inflammation without broadly suppressing pyroptosis suggest that IL-1β plays a dominant role in shaping inflammatory signaling in vivo, at least partially independent of pyroptosis-triggered DAMP release and its downstream signaling. Such functional uncoupling may be particularly relevant in tissues or disease settings where excessive cytokine release, rather than pyroptotic cell death, is the principal driver of the pathology.

Together, our findings establish ASC^{LD} as a previously unrecognized regulatory site that confers spatial control over IL-1β maturation. By directly recruiting pro-IL-1β and coordinating its processing, LD provides a mechanism to tune IL-1β output without altering inflammasome assembly or pyroptosis. This separation-of-function highlights an inherent modularity within inflammasomes and identifies a therapeutically actionable interface for selectively dampening IL-1β-driven pathology while preserving host protective inflammatory cell death.

Materials and Methods

Human HEK293T and THP-1 cells, as well as primary human monocyte-derived macrophages and peripheral blood mononuclear cells were used for inflammasomes assay. Primary human cells were derived from de-identified blood samples obtained from healthy donors. Cells were transfected with expression constructs encoding human NLRP3, ASC, caspase-1, and pro-IL-1β (IL1B), as depicted. THP-1 cells were differentiated and primed with lipopolysaccharide followed by activation with nigericin to induce NLRP3 inflammasome signaling. Cytokine release (IL-1β) was quantified by ELISA, and cell death was assessed by LDH release. Protein–protein interactions were assessed using NanoBRET and GST pull-down assays.

Confocal and fluorescence microscopy were used to assess ASC speck formation and subcellular localization. Stable cell lines were generated by lentiviral transduction where indicated. In vivo inflammasome activation was evaluated using mouse models of MSU- and LPS + ATP-induced peritonitis, followed by measurement of IL-1β levels and immune cell recruitment by flow cytometry.

Detailed experimental procedures, including cloning strategies, reagents, cellular imaging parameters, and full protocols, are provided in the *SI Appendix*.

Data, Materials, and Software Availability. All study data are included in the article and/or *SI Appendix*. Cell lines and reagents generated in this study are available from the corresponding author, V.G.M (vmagupalli@nybc.org), upon reasonable request and subject to scientific review and completion of a material transfer agreement.

ACKNOWLEDGMENTS. We thank Dr. Kate Fitzgerald (UMass Chan) for providing wild-type (WT) THP-1 cells and Dr. Daniel Bachovchin (MSKCC) for $ASC^{-/-}$ THP-1 cells. We are grateful to members of the Magupalli and Wu laboratories for insightful discussions. We thank Dr. Marc Rothenberg (CCHMC) for full-length (FL) human IL-33 plasmid and Dr. Cornelius Taabazuing (UPenn) for human caspase-1 (WT and mutant) plasmids. We thank Dr. Cheryl Lobo [New York Blood Center Enterprises (NYBCe)] for sharing healthy volunteer blood samples. We thank Zannatul Monia and Iris Erlanger at the NYBCe flow cytometry core facility, as well as Dr. Prem Yugandhar Kadiyam Sundarasivarao (Magupalli laboratory), for assistance with fluorescence-activated cell sorting (FACS) analysis, and Vijay Nandi, Head of data analytic services at NYBCe, for support with statistical analyses. We also thank Kathy Tang, Moises Custodio, and Fernando Ogando at the NYBCe Laboratory Animal Research Service (LARS) core facility. V.G.M acknowledges support from the Rose M. Badgeley Residuary Charitable Trust, National Institutes of Health (AR079766) and startup funds provided by the Lindsley F. Kimball Research Institute/NYBCe. H.S. is supported by faculty startup Grant from Khalifa University (FSU-2025-005). This work was supported by National Institutes of Health Grants R01HL155574 and R01HL135039 to L.L.L.; National Institutes of Health Grant K01 DK118041 and the Joslin Pilot and Feasibility Grant P30 DKO46200 (to I.S.); National Institutes of Health Grant R01 AI177778 (to H.W.) and a Breakthrough Type 1 Diabetes (Juvenile Diabetes research Foundation) Innovative Award (GRT66388) to I.S.

Author affiliations: [a]Laboratory of Molecular and Mechanistic Cell Signaling, Lindsley F. Kimball Research Institute, New York Blood Center, Rye, NY 10580; [b]Laboratory of Stem Cell Regenerative Research, Lindsley F. Kimball Research Institute, New York Blood Center, Rye, NY 10580; [c]Division of Endocrinology, Diabetes and Metabolism, Department of Medicine, Deaconess Medical Center and Harvard Medical School, Boston, MA 02115; [d]Department of Biological Sciences, College of Medicine and Health Sciences, Khalifa University, Abu Dhabi 127788, United Arab Emirates; [e]Department of Biological Chemistry and Molecular Pharmacology, Harvard Medical School, Boston, MA 02115; and [f]Program in Cellular and Molecular Medicine, Boston Children's Hospital, Boston, MA 02115

Author contributions: V.G.M. conceived the study, designed the experiments, and supervised the research; H.W. contributed to study conception and supervision; G.S., S.M., and V.G.M. designed and cloned constructs; P.A., G.S., and V.G.M. performed and analyzed NanoBRET studies; H.S. and V.G.M. conducted structure-based analysis and designed mutant constructs; G.S., R.W., P.A., and V.G.M. performed and analyzed cell-based assays; G.S., R.W., A.B., L.L.L., and V.G.M. performed and analyzed cellular imaging; G.S., I.S., and V.G.M. performed and analyzed in vivo experiments; and V.G.M. wrote the paper with input from H.W. and all authors.

1. K. V. Swanson, M. Deng, J. P. Ting, The NLRP3 inflammasome: Molecular activation and regulation to therapeutics. *Nat. Rev. Immunol.* **19**, 477–489 (2019).
2. K. C. Barnett, S. Li, K. Liang, J. P. Ting, A 360° view of the inflammasome: Mechanisms of activation, cell death, and diseases. *Cell* **186**, 2288–2312 (2023).
3. J. Yao, K. Sterling, Z. Wang, Y. Zhang, W. Song, The role of inflammasomes in human diseases and their potential as therapeutic targets. *Signal Transduct. Target. Ther.* **9**, 10 (2024).
4. T. Fernandes-Alnemri *et al.*, The pyroptosome: A supramolecular assembly of ASC dimers mediating inflammatory cell death via caspase-1 activation. *Cell Death Differ.* **14**, 1590–1604 (2007).
5. J. Masumoto *et al.*, ASC, a novel 22-kDa protein, aggregates during apoptosis of human promyelocytic leukemia HL-60 cells. *J. Biol. Chem.* **274**, 33835–33838 (1999).
6. F. L. van de Veerdonk, M. G. Netea, C. A. Dinarello, L. A. Joosten, Inflammasome activation and IL-1β and IL-18 processing during infection. *Trends Immunol.* **32**, 110–116 (2011).
7. J. Shi, W. Gao, F. Shao, Pyroptosis: Gasdermin-mediated programmed necrotic cell death. *Trends Biochem. Sci.* **42**, 245–254 (2017).
8. J. Shi *et al.*, Cleavage of GSDMD by inflammatory caspases determines pyroptotic cell death. *Nature* **526**, 660–665 (2015).
9. X. Liu *et al.*, Inflammasome-activated gasdermin d causes pyroptosis by forming membrane pores. *Nature* **535**, 153–158 (2016).
10. N. Kayagaki *et al.*, Caspase-11 cleaves gasdermin d for non-canonical inflammasome signalling. *Nature* **526**, 666–671 (2015).
11. K. Newton, A. Strasser, N. Kayagaki, V. M. Dixit, Cell death. *Cell* **187**, 235–256 (2024).
12. K. Newton, V. M. Dixit, N. Kayagaki, Dying cells fan the flames of inflammation. *Science* **374**, 1076–1080 (2021).
13. V. M. Dixit, The road to death: Caspases, cleavage, and pores. *Sci. Adv.* **9**, eadi2011 (2023).
14. H. K. De Jong *et al.*, Limited role for ASC and NLRP3 during in vivo *Salmonella* Typhimurium infection. *BMC Immunol.* **15**, 30 (2014).
15. P. Broz *et al.*, Redundant roles for inflammasome receptors NLRP3 and NLRC4 in host defense against *Salmonella*. *J. Exp. Med.* **207**, 1745–1755 (2010).
16. V. G. Magupalli *et al.*, HDAC6 mediates an aggresome-like mechanism for NLRP3 and pyrin inflammasome activation. *Science* **369**, eaas8995 (2020).
17. C. A. Dinarello, Overview of the IL-1 family in innate inflammation and acquired immunity. *Immunol. Rev.* **281**, 8–27 (2018).
18. P. Diaz-Parga, E. Alba, Inflammasome regulation by adaptor isoforms, ASC and ASCb, via differential self-assembly. *J. Biol. Chem.* **298**, 101566 (2022).
19. P. Diaz-Parga, A. Gould, E. Alba, Natural and engineered inflammasome adapter proteins reveal optimum linker length for self-assembly. *J. Biol. Chem.* **298**, 102501 (2022).
20. M. S. Dick, L. Sborgi, S. Rühl, S. Hiller, P. Broz, ASC filament formation serves as a signal amplification mechanism for inflammasomes. *Nat. Commun.* **7**, 11929 (2016).
21. N. B. Bryan *et al.*, Differential splicing of the apoptosis-associated speck like protein containing a caspase recruitment domain (ASC) regulates inflammasomes. *J. Inflamm. (Lond.).* **7**, 23 (2010).
22. D. Xue *et al.*, Atomic mechanisms of full-length ASC-mediated inflammasome assembly. *Nat. Commun.* **16**, 10564 (2025).
23. J. Jumper *et al.*, Highly accurate protein structure prediction with AlphaFold. *Nature* **596**, 583–589 (2021).
24. M. Varadi *et al.*, Alphafold protein structure database: Massively expanding the structural coverage of protein-sequence space with high-accuracy models. *Nucleic Acids Res.* **50**, D439–D444 (2022).
25. B. Yu, M. Blaber, A. M. Gronenborn, G. M. Clore, D. L. Caspar, Disordered water within a hydrophobic protein cavity visualized by x-ray crystallography. *Proc. Natl. Acad. Sci. U.S.A.* **96**, 103–108 (1999).

26. S. L. Vijayaraj *et al.*, The ubiquitylation of IL-1β limits its cleavage by caspase-1 and targets it for proteasomal degradation. *Nat. Commun.* **12**, 2713 (2021).
27. A. Lu *et al.*, Unified polymerization mechanism for the assembly of ASC-dependent inflammasomes. *Cell* **156**, 1193–1206 (2014).
28. D. Dong *et al.*, Inflammasome activity is controlled by ZBTB16-dependent SUMOylation of ASC. *Nat. Commun.* **14**, 8465 (2023).
29. P. R. Vajjhala *et al.*, The inflammasome adaptor ASC induces procaspase-8 death effector domain filaments. *J. Biol. Chem.* **290**, 29217–29230 (2015).
30. V. Sagulenko *et al.*, AIM2 and NLRP3 inflammasomes activate both apoptotic and pyroptotic death pathways via ASC. *Cell Death Differ.* **20**, 1149–1160 (2013).
31. D. Derossi, A. H. Joliot, G. Chassaing, A. Prochiantz, The third helix of the Antennapedia homeodomain translocates through biological membranes. *J. Biol. Chem.* **269**, 10444–10450 (1994).
32. M. R. Spalinger, M. Scharl, Mono sodium urate crystal-induced peritonitis for in vivo assessment of inflammasome activation. *Bio. Protoc.* **8**, e2754 (2018).
33. S. Mariathasan *et al.*, Cryopyrin activates the inflammasome in response to toxins and ATP. *Nature* **440**, 228–232 (2006).
34. F. Martinon, V. Pétrilli, A. Mayor, A. Tardivel, J. Tschopp, Gout-associated uric acid crystals activate the NALP3 inflammasome. *Nature* **440**, 237–241 (2006).
35. C. J. Chen *et al.*, MyD88-dependent IL-1 receptor signaling is essential for gouty inflammation stimulated by monosodium urate crystals. *J. Clin. Invest.* **116**, 2262–2271 (2006).
36. M. R. Spalinger *et al.*, NLRP3 tyrosine phosphorylation is controlled by protein tyrosine phosphatase PTPN22. *J. Clin. Invest.* **126**, 1783–1800 (2016).
37. I. I. Singer *et al.*, The interleukin-1 beta-converting enzyme (ICE) is localized on the external cell surface membranes and in the cytoplasmic ground substance of human monocytes by immuno-electron microscopy. *J. Exp. Med.* **182**, 1447–1459 (1995).
38. F. Martinon, K. Burns, J. Tschopp, The inflammasome: A molecular platform triggering activation of inflammatory caspases and processing of proIL-beta. *Mol. Cell* **10**, 417–426 (2002).
39. X. Liu *et al.*, Inflammasome-activated gasdermin d causes pyroptosis by forming membrane pores. *Nature* **535**, 153–158 (2016).
40. D. P. Cerretti *et al.*, Molecular cloning of the interleukin-1 beta converting enzyme. *Science* **256**, 97–100 (1992).
41. M. Monteleone *et al.*, Interleukin-1β maturation triggers its relocation to the plasma membrane for gasdermin-D-dependent and -independent secretion. *Cell Rep.* **24**, 1425–1433 (2018).